XIII Congresso Ibérico de Acústica
55º Congreso Español de Acústica
TECNIACÚSTICA 2024
Faro, 11 a 13 setembro 2024

BROADBAND PERFORMANCE OF MICRO-PERFORATED ACOUSTIC BLACK HOLES IN DUCTS

Teresa Bravo[1], Cedric Maury[2], Daniel Mazzoni[3], Muriel Amielh[3], Fawad Ali[2]

[1] Spanish National Research Council
e-mail: teresa.bravo@csic.es
[2] Laboratory of Mechanics and Acoustics (CNRS)
e-mail: cedric.maury@centrale-marseille.fr; fawad.ali@centrale-marseille.fr
[3] Institute of Research on Non-Equilibrium Phenomena (CNRS)
email: daniel.mazzoni@centrale-marseille.fr; muriel.amielh@univ-amu.fr

Resumen
El diseño de silenciadores compactos instalados en conductos para la atenuación de banda ancha en el margen de las bajas frecuencias es importante en sistemas de aire acondicionado, revestimientos de ventiladores o silenciadores de vehículos. Los agujeros negros acústicos (ABH) abiertos son una solución adecuada que atrapan y disipan ondas sonoras incidentes en un amplio margen de frecuencias al actuar simultáneamente sobre la transmisión y la reflexión sin impedir el flujo de aire. Inspirados en el concepto de agujeros negros de vibraciones, los ABH en conductos están formados por una distribución en serie de cavidades con espesores graduados que proporcionan un sonido retardado y una adaptación de impedancia. En este trabajo, se propone examinar la influencia de las interfaces microperforadas entre el conducto y las entradas a la cavidad para el rendimiento acústico del ABH. A partir de la formulación de la matriz de transferencia se demuestra que los microperforados amplían significativamente el rango de valores de disipación elevados en las bajas frecuencias. Los resultados obtenidos se han validado numéricamente con elementos finitos y experimentalmente en un banco de pruebas aeroacústicas con baja velocidad de flujo.

Palabras clave: agujeros negros acústicos, atenuación del sonido, absorción del sonido, microperfora.

Abstract
The design of compact duct silencers with broadband low-frequency attenuation performance is of importance for large diameters air conditioning systems, short turbofan liners or the exhaust mufflers of vehicles. Fully-opened acoustic black holes (ABH) in ducts are a suitable solution to trap and dissipate incident sound waves over a broad bandwidth. They can simultaneously stop the sound transmission and the back-reflections without blocking the air flow. Inspired by the concept of vibrational black holes, ducted ABHs are a serial distribution of graded cavity depths providing slow sound and impedance matching. In this work, it is proposed to examine the influence of micro-perforated interfaces between the duct and the cavity mouths on the ABH acoustical performance. It is shown from transfer matrix formulation that micro-perforates significantly extend the range of high dissipation values towards low-frequencies. The performance results are validated against finite element method and experiments carried out in a low-speed aeroacoustic test rig.

Keywords: acoustic black holes, sound attenuation, sound absorption, micro-perforates.

PACS nº. 43.50.-x, 43.50.+y

1 Introduction

The design of compact duct silencers with broadband low-frequency attenuation performance constitutes a permanent demand in the field of environmental noise control [1]. The use of passive materials is widely implemented and provides economical and efficient solutions for most of control problems in the mid and high frequency range [2]. However, more attention has been paid progressively to the low frequency content as an important number of noise sources present a preponderant contribution within the low frequency spectrum. This is especially important in the duct acoustic area with applications in ventilation and air conditioning systems, or in the field of transportation. Current acoustic devices for the reduction of major aircraft noise sources such as fan and jet noise are constituted of liners made up of a honeycomb core bonded to a perforated sheet in contact with the flow that acts as a resistive skin. Their performance is linked to the physical parameters that define the acoustic impedance and the architecture SDOF/ DDOF (single or double degree of freedom), bringing 3-4 EPNdB reduction on aircraft noise at each certification flight condition [3]. They have been used for decades and offer an excellent compromise in terms of performance, weight, structure and costs. However, new architectures of Ultra-High Bypass Ratio (UHBR) turbofans imply a lower blade passing frequency and a shorter nacelle with a reduced acoustic treatment surface. Surface transportation systems are also sources of low-frequency noise with prospective hybrid-electric and fully-electric propulsion systems in terms of low-frequency road noise transmitted inside the vehicles [4]. Considering limitations of classical noise control techniques, many attempts have recently tried to further improve the control using active control techniques [5]. They are well suited for the reduction of low-frequency noise in ducted systems downstream the secondary source position but they can also reinforce the primary field upstream [6]. Additionally, application in the field of aeroacoutics is still at an early stage. Taking stringent aviation safety conditions and energy consumption into consideration, active control methods are mainly applied to downscaled model and have moderate Technology Readiness Level for implementation in real situations.

Micro-Perforated Panels (MPPs) have been proposed for applications in demanding environments where classical porous or fibrous solutions cannot be used. Maa [7, 8] developed the theory for MPPs with diameter perforations of sub-millimeters, and they have been widely used in architectural acoustics and noise control engineering design [9]. They can be manufactured from different materials such as cardboard, plastic or plywood, constituting an ecological and recyclable option for light and soundproof solutions. They can also be designed according to specific absorption characteristics by the proper optimization of the physical constitutive parameters, that makes them flexible tuned absorbers. In particular, they have been studied as mufflers in air-flow ducts [10, 11] working under linear and non-linear excitations [12]. Although they provide important attenuation values, these are confined to a narrow frequency band that normally does not exceed two octaves. Multi-layer configurations, with different parameters for holes diameters, perforation ratio and panel thickness can be used to improve the sound absorption bandwidth but at the expense of the increase of the total thickness of the sound absorber [13, 14]. Also, it has been shown that increasing the number of partitions in the cavity, a wide uniform range of absorption can be attained but maximum absorption would be dropped [15]. Use of combinations of series or parallel absorbers arrays then presents a trade-off between maximum absorption coefficient and wide-band performance.
Acoustic metamaterials have appeared recently with applications in many areas including broadband attenuation of sound in the low frequency range [16]. The interaction with these materials can alter and manipulate the natural characteristics of the incident wave field. The objective is to create a structural building block that, when assembled into a larger sample, exhibits the desired values of the key effective parameters, the mass density and the bulk modulus [17]. In this work, we will make use of the “slow sound” generation when acoustic waves propagate in a ducted flow surrounded by a

metamaterial. If the effective velocity of the incoming sound wave is progressively reduced to zero, a non-reflecting edge condition can be realized [18] and sound waves can be eventually confined in the meta-structure. This new concept has been denoted as an Acoustic Black Hole (ABH) and presents great potential for acoustic energy trapping.

The idea of energy confining by retarding structures was primarily developed in the field of vibration control and implemented by Mironov [19] in a in a beam structure with a tapped termination based on a power-law thickness profile. It was experimentally verified with a series of rigid discs fixed on a rod with their diameters progressively decreasing according to a parabolic law [20]. The Vibrational Black Hole prevented reflection of the waves when reaching the end of the structure. The noise control application for attenuation of the sound propagating along a waveguide has been considered more recently. ABHs constitute a category of retarding structures induced by a power law decay of the wave velocity in the fluid domain [21]. Initially, they aimed at minimization of reflection from a closed-end duct to achieve perfect anechoic terminations. An analytical description in terms of the Transfer Matrix Method [22] has helped to make a great advancement for the prediction of the absorption of linear or quadratic ABHs. Numerical simulations have also shown that the primary source of damping, e.g. visco-thermal dissipation in the ABH cavities, is responsible for a low reflection coefficient over the ABH bandwidth, but it could be enhanced at all frequencies by adding a small layer of damping material at the end of each cavity close to the outer ring [23]. Zhang and Cheng [24] added damping by introducing micro-perforated inner facings that considerably extended towards low frequencies the bandwidth of closed and open-ended ABHs.

The study of open-ended ABHs has been developed in the last years for systems that have to be flow-compliant. For this problem, the goal is to consider both minimization of reflection and transmission for the open muffler without impeding the circulation of the axial flow. For the open-ended arrangement, it has been demonstrated that good performance in the dissipated power can be achieved above $k_0 L = 2.5$ [18]. However, to extend their efficiency in the low frequency range, the presence of coating material such as MPPs could be included. The objective of this work is to enhance the visco-thermal dissipation mechanisms through the inclusion of micro-perforations at the entrance of the resonant cavities with axially graded depth. This micro-perforated facing will also shield the acoustic treatment from an eventual flow through the low-drag micro-structured interface, reducing the pressure drop of the wall-treatment and keeping a nominal flow rate. An analytical model is presented in Section 2 to show the occurrence of slow-sound effects inside an open-ended ABH. This model will be assessed in Section 3 against a numerical approach and will be used consequently to perform a parametric study on the dissipative performance of the metamuffler, leading to optimal values of the MPP coating that enhance the total dissipation. Section 4 will present experimental results of a rectangular ABH with perforated coating in the no-flow case, that will be assessed against numerical results. We will then proceed with the main conclusions and guidelines for further works.

2 Acoustic performance of the ABH muffler

2.1 Micro-perforated panel transfer impedance

We investigate ABH acoustic properties for sound dissipation in a duct by considering the system sketched in Figure 1. It is composed of a set of rings separated by air cavities with a constraint on the maximum length L along the axial direction not to exceed 0.15 m. The outer rings radii increase progressively according to a power law. The ABH muffler is inserted in a perfectly hard tube section with constant radius R. The silencer extends from the inlet (short cavities) situated at $z = -L$ to the outlet (deep cavities) at $z = 0$, as shown in Figure 1.

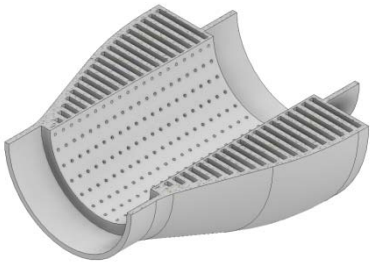

Figure 1- Diagram of a cylindrical ABH muffler where the cavity rings of increasing depth are connected to the main duct by a micro-perforated facing.

The novelty with this design is the addition of a micro-perforated facing between the muffler and the inner duct that provides additional damping and inertia to extend the muffler performance towards the low frequency range. It is assumed that an acoustic plane wave ($e^{j\omega t}$) propagates downstream in the duct, especially in the ABH section lined by a uniform coating composed of a micro-perforated cylindrical panel. The overall transfer impedance, Z_{MPP}, for the MPP with circular holes of diameter d_h and thickness t_h is given by the following expression [7, 8]

$$\frac{Z_{\mathrm{MPP}}}{\sigma}=\frac{32\eta t_h}{\sigma d_h^2}\left[\sqrt{1+\frac{k_h^2}{32}}+\frac{\sqrt{2}}{32}k_h\frac{d_h}{t_h}\right]+\mathrm{j}\rho_0\omega\frac{t_h}{\sigma}\left[1+\left(9+\frac{k_h^2}{2}\right)^{-1/2}+\frac{8}{3\pi}\frac{d_h}{t_h}\right], \tag{1}$$

with σ the perforation ratio, η the dynamic viscosity of the air, and $k_h=(d_h/2)/r_{\mathrm{visc.}}(\omega)$, the perforate constant, e.g. the ratio of the holes radius to the viscous boundary layer thickness, $r_{\mathrm{visc.}}(\omega)=\sqrt{\eta/\rho_0\omega}$, with ρ_0 the air density. This impedance, when $k_h<<1$, can be approximated by

$$\frac{Z_{\mathrm{MPP}}}{\sigma}=\frac{At_h}{\sigma d_h^2}+\mathrm{j}\rho_0\omega\frac{t_h}{\sigma}, \tag{2}$$

with $A=2.2\times 32\eta$, this expression being valid for linear acoustic regimes. The behavior of MPP partitions has been studied before for in-duct geometries [12] and in presence of a mean flow.

2.2 ABH analytical formulation

The equation that governs the behavior of a plane wave travelling along a ducted geometry lined by a fully-opened ABH muffler with total length L and radius R has been outlined assuming an infinite number of cavities separated by infinitely thinned walls.

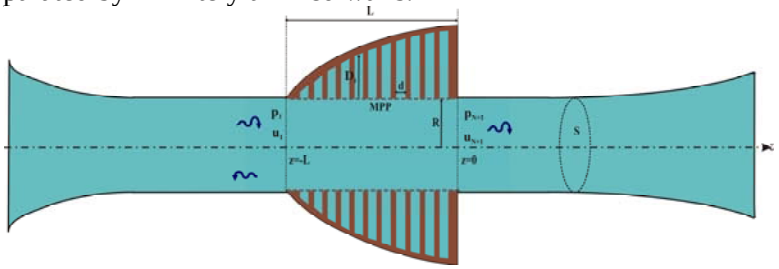

Figure 2- Two-dimensional view of the ABH metamuffler and the physical quantities involved.

The linearized mass conservation equation can be written as

$$\frac{\partial v_z}{\partial z}+\frac{v_n}{r_H}+\frac{\mathrm{d}(\log S)}{\mathrm{d}z}v_z=-\frac{\mathrm{j}\omega}{\rho_0 c_0^2}p,\quad -L<z<0\,, \tag{3}$$

with v_z the axial velocity component, $v_n=p/Z$ the normal velocity over the boundary $\Sigma(r=R,-L<z<0)$ and p the acoustic pressure. $r_H=S/U$ is the hydraulic radius with S the cross-sectional area of the duct and U the circumference of the lining.

Equation (3) can be simplified considering that for a fully-opened ABH with a constant radius, $\mathrm{d}(\log S)/\mathrm{d}z=0$. Applying the linearized momentum conservation equation, $-\mathrm{j}\omega\rho_0 v_z=\partial p/\partial z$, it leads to a modified Helmholtz-type equation of the form

$$\frac{\mathrm{d}^2 p}{\mathrm{d}z^2}+k_0^2\left[1-\mathrm{j}\frac{y(z)}{k_0 r_H}\right]p=0\,. \tag{4}$$

with $k_0=\omega/c_0$ the acoustic wavenumber and $y(z)=Z_0/Z(z)$ the wall specific admittance that varies along the axial duct direction, normalised by $Z_0=\rho_0 c_0$ the fluid characteristic impedance with ρ_0 the air density and c_0 the sound speed. For a locally-reacting ABH made up of a continuous distribution of annular cavities with axially varying depth $D(z)$ and neglecting the visco-thermal losses in the cavities, the wall-admittance at the cavity mouths is given by [21]

$$y(z)=-\mathrm{j}\frac{J_1(k_0R)H_1[k_0(R+D(z))]-J_1[k_0(R+D(z))]H_1(k_0R)}{J_0(k_0R)H_1[k_0(R+D(z))]-J_1[k_0(R+D(z))]H_0(k_0R)}, \tag{5}$$

with J_1 and H_1 Bessel and Hankel functions of the first kind. An approximation to Equation (5) can be obtained in the low frequency range. When $k_0R<<1$, Equation (5) simplifies into

$$y(z)=\mathrm{j}k_0\left[R^2-(R+D(z))^2\right]\,, \tag{6}$$

an axial distribution of stiffness-like admittance. Let us now assume that the ABH is coated in the waveguide by a micro-perforated lining. One obtains from the combination of Equation (2) and Equation (6) the following wall admittance,

$$y(z_i)=\left[\frac{At_h}{Z_0\sigma d_h^2}+\mathrm{j}\left(\frac{\omega t_h}{\sigma c_0}-\frac{1}{k_0\left[D+D^2/2R\right]}\right)\right]^{-1}\,. \tag{7}$$

Considering that a progressive increase of the ABH cavity depths along the axial coordinate can be expressed mathematically as $D(z)=R(1-\varphi_m(z))$, with $\varphi_m(z)=(-z)^m/L^m, m>0$, and substituting it into Equation (4), we get a Helmholtz-type equation,

$$\frac{\mathrm{d}^2 p}{\mathrm{d}z^2} + \frac{\omega^2}{c_z^2} p = 0, \tag{8}$$

where

$$\frac{\omega^2}{c_z^2} = k_0^2 \left\{ 1 - \mathrm{j} \frac{Z_0 \sigma^2 d_h^2 c_0 \left[D + D^2/2R \right]}{A t_h \sigma c_0 k_0 (D/2) \left[R + D/2 \right] + j Z_0 \sigma d_h^2 B} \right\}, \tag{9}$$

with $B = \omega t_h k_0 \left(R + D/2 \right) D/2 - \sigma c_0 \left(R/2 \right)$ and the following values of the phase velocity at the ABH inlet ($z = -L$) and outlet ($z = 0$)

$$c_z = \begin{cases} c_0 & \text{for } z = -L \\ c_0 \left[\dfrac{\omega t_h k_0 \dfrac{3R}{4} - \dfrac{\sigma c_0}{2}}{\omega t_h k_0 \dfrac{3R}{4} - 2\sigma c_0} \right]^{1/2} & \text{for } z = 0. \end{cases} \tag{10}$$

where the MPP resistance A has been neglected for simplification purposes.

One now considers a cylindrical ABH muffler with maximum cavity depth 0.047 m, increase rate of the cavities depth $m = 2$ lining a duct of radius 0.047 m over an axial length $L = 0.1\,\mathrm{m}$. The MPP has holes diameter of 0.8 mm, thickness of 0.5 mm and a perforation ratio of 2%. One observes from Fig. 3 that the inertial effect of the MPP over the ABH cavities with graded cavity depths further reduces the acoustic phase velocity from $c_0/2$ (slow sound without MPP) down to zero over the efficiency range of the MPP-coated ABH muffler, e.g. over 1300 Hz – 2000 Hz. Meanwhile, the attenuation driven by the imaginary part of the phase velocity becomes non-zero valued above 1300 Hz at the onset of the ABH efficiency range.

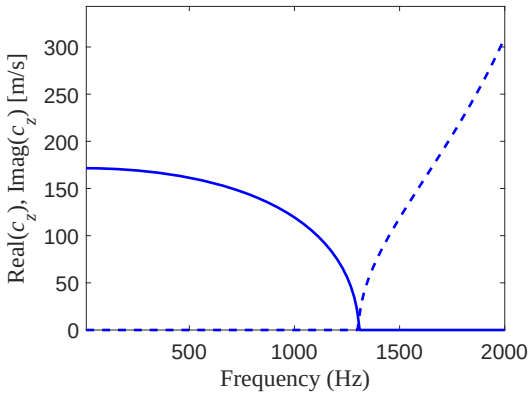

Figure 3-Propagative (plain) and attenuation (dashed) terms for the axial phase velocity at the outlet of the ABH muffler calculated from Equation (10).

2.3 Transfer Matrix Method

The Transfer Matrix Method (TMM) is an analytical method that models the propagation of acoustic waves through a stratified medium. The TMM can be used to describe the wave propagation within an ABH muffler when considering a finite number N of annular cavities of width d , separated by rigid

rings of finite thickness d_t. The cavity depths can be discretized as $D_i = R(1-\varphi_m(z_i))$ with $i = 1,...,N$ and $m > 0$. The input impedance associated to an uncoated side-branch cavity of depth D is given by $Z_{\text{cav}} = -\text{j}(Z_0/S_{\text{cav}})\cot(k_0 D)$, that can be approximated in the low frequency range as $Z_{\text{cav}} = -\text{j}(Z_0/S_{\text{cav}})(k_0 D)^{-1}$. It is associated to the local side-branch volume admittance given by $Y_{\text{cav},i} = S_{\text{cav}} y(z_i)/Z_0$ with $S_{\text{cav}} = 2\pi R d$ the cavity entrance area and $y(z_i)$ provided by Equation (7) when considering plane-wave propagation in the duct and the adjacent cavities. Whether the cavity is mounted directly onto the duct or is coated by a MPP lining, it takes the expression

$$Y_{\text{cav},i} = \begin{cases} \text{j}\dfrac{k\pi d}{Z_0}\left[(R+D_i)^2 - R^2\right] & \text{without MPP} \\ c_0\left[\dfrac{Z_{Maa}}{S_{\text{cav,i}}} - \text{j}\dfrac{Z_0}{k\pi d\left[(R+D_i)^2 - R^2\right]}\right]^{-1} & \text{with MPP} \end{cases} \tag{11}$$

To calculate the acoustic performance of the fully-opened ABH, continuity conditions are applied on the acoustic pressure $(p_i = p_{i+1})$ and on the acoustic flow rate $(u_i = (p_{i+1}/Z_{cav}) + u_{i+1})$ at the i^{th} cavity-ring unit. One then obtains a relationship between the input and output quantities at the i^{th} interface that reads $[p_i \; u_i]^{\text{T}} = \mathbf{T}_i[\text{p}_{i+1} \; u_{i+1}]^{\text{T}}$, with the following elementary transfer matrix

$$\mathbf{T}_i = \begin{bmatrix} \cos(k_0 d) & \text{j}\dfrac{Z_0}{S}\sin(k_0 d) \\ \text{j}\dfrac{S}{Z_0}\sin(k_0 d) & \cos(k_0 d) \end{bmatrix} \begin{bmatrix} \cos(k_0 d_t) & \text{j}\dfrac{Z_0}{S}\sin(k_0 d_t) \\ \text{j}\dfrac{S}{Z_0}\sin(k_0 d_t) & \cos(k_0 d_t) \end{bmatrix} \begin{bmatrix} 1 & 0 \\ Y_{\text{cav},i} & 1 \end{bmatrix}. \tag{12}$$

The total transfer matrix between the ABH inlet and outlet, is calculated as the product of the elementary sub-matrices associated at each unit as

$$\mathbf{T} = \prod_{i=1}^{N} \mathbf{T}_i = \begin{bmatrix} T_{11} & T_{12} \\ T_{21} & T_{22} \end{bmatrix}. \tag{13}$$

Imposing the plane wave continuity conditions, $p_{N+1} = Z_0 u_{N+1}/S$, at the output of the ABH muffler, we obtain the following expressions for the reflection and transmission coefficient in terms of the particular elements of the overall transfer matrix $\mathbf{T}$ as

$$\begin{cases} r = \dfrac{(T_{11} + z_0 T_{12}) - (T_{21} + z_0 T_{22})}{(T_{11} + z_0 T_{12}) + (T_{21} + z_0 T_{22})}, \\ t = \dfrac{1+r}{T_{11} + z_0 T_{12}} \end{cases} \tag{14}$$

with $z_0 = S/Z_0$. The power dissipated by the ABH can be calculated as $\eta = 1 - |r|^2 - |t|^2 = \alpha - \tau$ with α the absorption coefficient and τ the transmission coefficient. The transmission loss (TL) is obtained from the transmission coefficient as $\text{TL(dB)} = -10\log_{10}(\tau)$.

3 Prediction of the ABH dissipative performance

3.1 FEM analysis

The proposed analytical TMM has been evaluated against a numerical finite element (FEM) approach. For a better comparison, we have considered the visco-thermal losses within the cavities and the duct fluid domains using the Johnson-Champoux-Allard-Lafarge (JCAL) model [25], expressed as a function of complex acoustic wavenumbers $k_0' = \omega\sqrt{\rho_{d,c}(\omega)C_{d,c}(\omega)}$ and impedances $Z_0' = \omega\sqrt{\rho_{d,c}(\omega)C_{d,c}^{-1}(\omega)}$ in the transfer matrices of Equation (12), with $\rho_{d,c}(\omega)$ the effective density that describes the visco-inertial effects and $C_{d,c}(\omega)$ the air compressibility that accounts for the thermal effects. The JCAL parameters have been selected considering the related literature [24]. Comsol Viscothermal Acoustics has been used as a benchmark to check the TMM analytical predictions. An infinite length duct has been mimicked by imposing perfectly matched layers boundary conditions at the inlet and outlet duct sections to avoid back-reflected waves. Quadratic elements have been used for the pressure, velocity and temperature fields for a 2D axisymmetric simulation. Care has been taken to ensure that the maximum element size, set to $d/3$, was able to ensure that at least ten nodal points per acoustic wavelength were generated at the first cut-on frequency of the waveguide, that constitutes the highest frequency of interest in this configuration. Attention has also been paid to well resolve the visco-thermal boundary layers along the ABH rings and duct walls.

The physical parameters considered for the simulations have been selected from those typically considered for fully-opened ABH geometries presented in the literature [21]. They correspond to a duct radius $R = 0.047\,\text{m}$, that provides a cut-on frequency $f_c \approx 1.84 c_0/(2\pi R) = 2142\,\text{Hz}$, and an ABH axial length $L = 0.1\,\text{m}$. The ABH muffler is constituted of $N = 15$ annular cavities of axial width $d = 0.004\,\text{m}$ separated by ring walls of thickness $d_t = 0.0027\,\text{m}$, thus leading to a wall porosity $\sigma = d/(d + d_t) = 60\,\%$ over the silencer section. The axial rate at which the cavity depths increase is chosen as $m = 2$. The micro-perforated cylindrical coating has been selected with a thickness of $t_h = 0.5$ mm, circular holes of diameter $d_h = 0.5\,\text{mm}$ and a perforation ratio of 10%. The results for the dissipated, reflected and transmitted powers are presented in Figure 4.

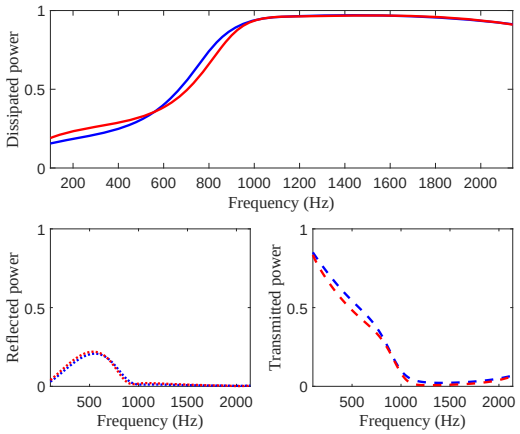

Figure 4- Comparison between the simulated ABH acoustical performance when calculated with the TMM (blue) and FEM (red): dissipated (plain), reflected (dotted) and transmitted (dashed) powers.

It can be seen that the agreement between the analytical TMM predictions and those obtained with the FEM code agree reasonably well within the frequency range of interest. This validates the simplified TMM and makes it suitable to be used for a parametric study and selection of the optimal parameters with an affordable computational time. It can be also appreciated that the proposed ABH-type muffler presents values of dissipation exceeding 0.6 above 700 Hz, although an optimal efficiency range can be achieved between 1 kHz and 1.8 kHz, with a dissipation value that exceeds 0.9. Meanwhile, the reflection (resp. transmission) coefficients does not exceed 0.01 (resp. 0.02) over the MPP-coated efficiency range, confirming the ABH-effect.

3.2 Selection of the physical constitutive parameters

Due its high number of parameters, the proposed ABH muffler constitutes a tunable control device that can be adjusted to achieve optimal performance considering different criteria. Particle swarm optimization [26] of the ABH and MPP parameters has been achieved to maximize the total dissipated power between 100 Hz and 2000 Hz, leading to the red curve in Figure 5.

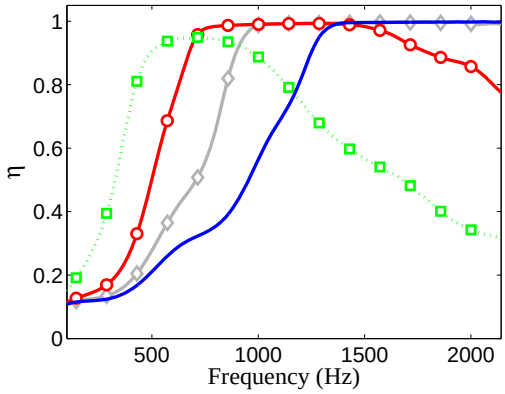

Figure 5- Acoustic power dissipated by the ABH cylindrical muffler when mounted on a waveguide (no MPP coating, blue) and when coated by a micro-perforated liner with different holes diameters: $d_h = 0.6$ mm (green), $d_h = 1.3$ mm (red) and $d_h = 3$ mm (grey).

One clearly shows the downshift of the onset frequency for the ABH muffler from 1400 Hz in the uncoated case down to 700 Hz with MPP coating. This is due to added inner and outer inertial effects induced by the MPP apertures on the individual MPP-cavity resonances. The resistivity due to the MPP holes adds up to the visco-thermal dissipation inside the cavities. It still maintains a balanced loss-to-leakage ratio for holes diameter down to $d_h = 1.3$ mm but, for smaller holes, the losses exceed the leakage due to a too high added flow resistivity at the MPP apertures. The maximum dissipation value then decays while it occurs at lower frequencies. A similar trend was observed when increasing the MPP holes pitch.

4 Experimental set-up

A rectangular ABH muffler of length, height and width of 0.15 m, made up of 20 cavities of width 0.0035 m, separated by walls of thickness 0.004 m, whose depth increases at a rate $m = 2$, has been

manufactured in ABS polymer using fused deposition modelling. A square cross-section was chosen to comply with the upstream and downstream square duct sections into which the muffler was inserted. Figure 6 shows that the ABH muffler is coated by perforations of diameter 2 mm, thickness 1 mm and perforation ratio 7%. Its scattering matrix is measured below the first duct cut-on frequency (1143 Hz) using the two-sources method [27] and two ¼ inch condenser microphones separated by 0.05 m, located upstream and downstream of the test section. One could then deduce the acoustic power dissipated, reflected and transmitted by the ABH muffler with perforated coating, as shown in Figure 6.

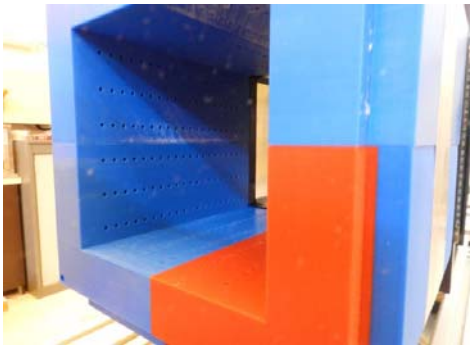

Figure 6- Photograph of the square ABH muffler with a perforated lining.

Numerical finite element calculation of the ABH acoustical performance has been performed with Comsol and compared to that measured in the waveguide. One consistently observes in Figure 7 from both model and measurements that the ABH efficiency range (with a dissipation greater than 0.95) only occurs between 700 Hz and 800 Hz due to non-optimized MPP and ABH parameters. The added inertial effect of the perforated coating is responsible for the shift down to 730 Hz of the maximum dissipation value, that would otherwise occur at higher frequencies if not coated. The measured dissipation over (resp. under-) estimates that calculated above (resp. below) 730 Hz. It is likely related to the internal porosity and surface roughness of the polymer that respectively enhances the added resistivity and modified the viscous boundary layer thickness.

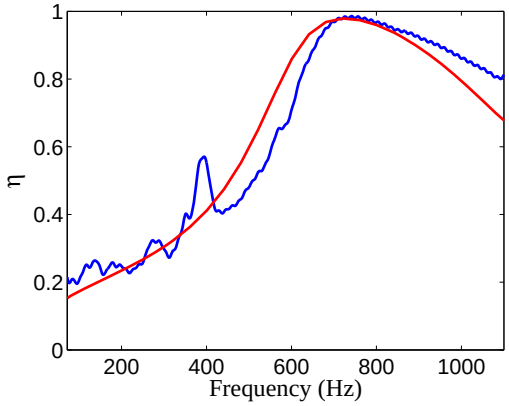

Figure 7- Acoustic power dissipated by the coated ABH muffler: calculated by FEM (red) and determined experimentally (blue).

5 Conclusions

A MPP-coated ABH muffler is proposed that is able to achieve both low reflection, low transmission and high dissipation over a broad bandwidth. The key mechanisms are impedance matching and merging of the cavities individual resonances. The MPP coating achieves a suitable added resistivity able to compensate for the inertial or stiffness leakages so that the incident wave is trapped and dissipated inside the ABH structure over a wideband efficiency range. Slow sound effects and wave attenuation are shown to be effective, especially over the efficiency bandwidth of the ABH. TMM and FEM models have shown to consistently predict the acoustical performance of MMP-coated ABH mufflers. In particular, lowering the MPP holes diameter or perforation ratio shifts the ABH muffler efficiency range towards the low-frequencies. An optimal value of the MPP holes diameter has been found from particle swarm algorithm below which the losses exceed the leakages.

The predicted FEM acoustical performance compared reasonably well against those measured in a transmission tube on a 3D printed ABH muffler. The correlation could however be improved if the muffler parameters were characterized and accounted for in the ABH optimization process in order to achieve a robust design of ABH muffler from cost-effective additive manufacturing. On-going studies incorporate the effect of a mean grazing flow into the models and experiments are being performed in a low-speed wind-tunnel to assess the sensitivity of the ABH effect to upstream or downstream flow conditions.

Acknowledgements

This work is part of the project TED2021-130103B-I00, funded by MCIN/AEI/10.13039/501100011033 and the European Union “Next Generation EU”/PRTR, and project PID2022-139414OB-I00 funded by MCIN/AEI/10.13039/501100011033/ and by "ERDF A way of making Europe". It has also received support from the French government under the France 2030 investment plan, as part of the Initiative d'Excellence d'Aix-Marseille Université - A*MIDEX (AMX-22-RE-AB-157). The authors are grateful to E. Bertrand for their technical and experimental support during the wind-tunnel testing at IRPHE Laboratory.

References

[1] Bies, D.A., Hansen, C.H., Howard, C.Q. & Hansen, K.L. (2023). *Engineering Noise Control,* Taylor & Francis Group, LLC, Boca Raton, USA.
[2] Fuch, H. (2013). Applied Acoustics: Concepts, Absorbers, and Silencers for Acoustical Comfort and Noise Control, Springer-Verlag, Berlin, Germany.
[3] Mercat, F. (2021). Nacelle acoustic liners desing and integration in aircraft environment, Workshop *DOCCLA*, Onera, Bordeux, France, 14-17 June 2021.
[4] Yu, Z., Cheng D. & Huang, X. (2019). Low-Frequency Road Noise of Electric Vehicles Based on Measured Road Surface Morphology, *World Electric Vehicle Journal*, Vol. 10(2), 33.
[5] Hansen, C.H. (2001). Understanding Active Noise Control Cancellation, *Spon Press*, London, U.
[6] Hansen, C.H. & Hansen, K.L. (2022). Noise Control, from concept to application, *CRC Press*, Taylor and Francis Group, Oxon, United Kingdom.
[7] Maa, D. Y. (1998). Potential of microperforated panel absorbers, *Journal of the Acoustical Society of America*, Vol. 104, 2861–2866.
[8] Maa, D. Y. (1997). Microperforated-panel wideband absorbers, *Noise Control Engineering Journal*, Vol. 29, 77–84.

[9] Kang, J. & and Fuchs, H.V. (1999). Predicting the absorption of open weave textiles and micro-perforated membranes backed by an air space, *Journal of Sound and Vibration*, Vol. 220, 905–920.
[10] Allam, S. & Åbom, M. (2011). A New Type of Muffler Based on Microperforated Tubes, *ASME Journal of Vibration and Acoustics* Vol. 133, 1–8.
[11] Maury, C., Bravo, T. & Mazzoni, D. (2019). The use of micro-perforations to attenuate the cavity pressure fluctuations induced by a low-speed flow, *Journal of Sound and Vibration*, Vol. 439, 1-16.
[12] Bravo, T., Maury, C. & Pinhede, C. (2016). Optimisation of micro-perforated cylindrical silencers in linear and nonlinear regimes, *Journal of Sound and Vibration*, Vol. 363, 359–379.
[13] Bravo, T., Maury, C. & Pinhede, C. (2013). Enhancing sound absorption and transmission through flexible multi-layer micro-perforated structures, *Journal of the Acoustical Society of* America Vol. 134 (5), 3663–3673.
[14] Sakagami, K., Morimoto, M. & Koike, W. (2006) A numerical study of double-leaf microperforated panel absorbers, *Applied Acoustics*, Vol. 676, 609–619.
[15] Wang, C. & and Huang, L.H. (2011). On the acoustic properties of parallel arrangement of multiple micro-perforated panel absorbers with different cavity depths, *Journal of the Acoustical Society of America* Vol. 130(1), 208-218.
[16] Cummer, S.A., Christensen, J. & and Alu, A. (2016). Controlling sound with acoustic metamaterials, *Nature Reviews*, 16001, 1-13.
[17] Ma, G. & and Sheng, P. (2016). Acoustic metamaterials: From local resonances to broad horizons, *Science Avances*, Vol. 2, 1-16.
[18] Mi, Y., Zhai, W., Cheng, L., Xi, C. & Yu, X. (2021). Wave trapping by acoustic black hole: Simultaneous reduction of sound reflection and transmission, *Applied Physics Letters* Vol. 118 (11), 114101.
[19] Mironov, M.A. & Pislyakov, V.V. (2002). One-Dimensional Acoustic Waves in Retarding Structures with Propagation Velocity Tending to Zero, *Acoustical Physics* Vol. 48: 347–352.
[20] Mironov, M.A. & Pislyakov, V.V. (2020). One-Dimensional sonic black holes: Exact analytical solution and experiments, *Journal of Sound and Vibration* 473, 347–352.
[21] Bravo, T. & Maury, C. (2023). Broadband sound attenuation and absorption by duct silencers based on the acoustic black hole effect: Simulations and experiments, Journal of Sound and Vibration, Vol. 561, 117825.
[22] Guasch, O., Sánchez-Martín & P., Ghilardi, D. (2020). Application of the transfer matrix approximation for wave propagation in a metafluid representing an acoustic black hole duct termination, *Applied Mathematical Modelling* Vol. 77, 1881–189.
[23] Mousavi, A., Berggren, M. & Wadbro, E. (2022). How the waveguide acoustic black hole works: A study of possible damping mechanisms, *Journal of the Acoustical Society of America* 151 4279–4290.
[24] Zhang, X. & Cheng, L. (2021). Broadband and low frequency sound absorption by Sonic black holes with Micro-perforated boundaries, *Journal of Sound and Vibration* 512, 116401.
[25] Champoux, Y. & and Allard, J.F. (1991). Dynamic tortuosity and bulk modulus in air-saturated porous media, *Journal of Applied Physics*, Vol. 70, 1975–1979.
[26] Parsopoulos, K: & Vrahatis, M. (2002). Recent approaches to global optimization problems through Particle Swarm Optimization, *Natural Computing*, Vol. 116, 235-3063.
[27] Lavrentjev, J., Åbom, M. & Bodén, H. (1995). A measurement method for determining the source data of acoustic two-port sources, *Journal of Sound and* Vibration, Vol. 183, 517–531.